metals

MDPI

Article

Novel Cast and Wrought Al-3Zn-3Mg-3Cu-Zr-Y(Er) Alloys with Improved Heat Resistance

Maria V. Glavatskikh, Ruslan Yu. Barkov, Leonid E. Gorlov, Maxim G. Khomutov and Andrey V. Pozdniakov *

Department of Physical Metallurgy of Non-Ferrous Metals, NUST MISIS, 119049 Moscow, Russia; glavatskikh@edu.misis.ru (M.V.G.); barkov@misis.ru (R.Y.B.); m1803226@edu.misis.ru (L.E.G.); khomutov@misis.ru (M.G.K.)

* Correspondence: pozdniakov@misis.ru

Abstract: The main weaknesses of commercial high-strength Al-Zn-Mg-Cu-based alloys are the low casting properties, corrosion and heat resistance. Al-Zn-Mg-Cu-based alloys with Zn/Mg ratio equal to 1 combine good strength, corrosion and heat resistance. Al alloys with atomic ratio Cu/Y(Er) equal to 4 have a narrow solidification range and high solidus temperature. Two basic principles were taken into consideration to develop novel heat-resistant Al-Zn-Mg-Cu-based alloys with improved casting properties: 1—mass ratio of Zn/Mg = 1, and 2—atomic ratio of Cu/Y(Er) = 4. The microstructure, phase transformation and tensile properties of the novel cast and wrought Al–3Zn–3Mg–3Cu–0.2Zr–Y(Er) alloys were investigated. The structure and phase composition were investigated via thermodynamic calculation, optical and scanning electron microscopy and X-ray diffraction methods. A two-step solution treatment with higher temperature in the second step provides a microstructure with better elongation, making possible to increase the hot rolling temperature of the Y or Er-containing alloys. The yield strength (YS) of the alloys decreased insignificantly from 270 to 290 MPa at room temperature to 225 to 260 MPa at 200 °C after casting, solution treatment, water quenching and aging. A better combination of the YS = 291–345 MPa and elongation (El.) (11–14.8%) was achieved in the Al3Zn3Mg3CuY and Al3Zn3Mg3CuEr alloys after solution treatment, rolling, recrystallization annealing, water quenching and aging compared with the Al3Zn3Mg3Cu alloy with YS = 245–340 MPa and El. = 6.8–12.5%.

Keywords: aluminum alloys; microstructure; mechanical properties; precipitates; erbium; yttrium

Citation: Glavatskikh, M.V.; Barkov, R.Y.; Gorlov, L.E.; Khomutov, M.G.; Pozdniakov, A.V. Novel Cast and Wrought Al-3Zn-3Mg-3Cu-Zr-Y(Er) Alloys with Improved Heat Resistance. *Metals* **2023**, *13*, 909. https://doi.org/10.3390/met13050909

Academic Editors: Frank Czerwinski and Noé Cheung

Received: 11 April 2023
Revised: 4 May 2023
Accepted: 5 May 2023
Published: 8 May 2023

1. Introduction

Al-Zn-Mg-Cu-based compositions are part of the high-strength wrought Al alloys. The compositions of this wrought Al alloy group were developed to achieve the highest strength and impact strength. The basic weaknesses of the Al-Zn-Mg-Cu-based alloys are the low casting properties, corrosion and heat resistance [1–4]. The cast Al-Zn-Mg-Cu alloys of the 7xxx series have the same flaws [5,6]. The main way to improve the casting and high-temperature properties is alloying with eutectic forming elements [7–14]. On the other hand, Al-Zn-Mg-Cu-based alloys with a Zn/Mg ratio near 1 combine good strength, corrosion and heat resistance [2–5,13,14]. Trace amounts of rare earth scandium or zirconium improve the room- and high-temperature strength and casting properties due to $L1_2$-precipitate formation during annealing and grain refining during solidification [14–18]. However, Sc is a very high-cost additive in Al alloys. In this case, the search for an adequate substitution of scandium in Al alloys is an important task. Titanium, yttrium and erbium in combination with zirconium provide the same effect in strengthening Al due to nucleation of the $L1_2$-precipitates [19–29]. Titanium [19–22], erbium [23–28] and yttrium [29] substitute the Zr atoms in the Al_3(Zr,Me) (Me=Ti,Y, or Er) precipitates. Titanium addition does not improve the coarsening resistance of the ternary alloy at temperatures of 375–425 °C [20]. However, Ti reduces the incubation time for nucleation and also increases

the peak hardness achieved during aging at temperatures of 450–600 °C [21]. The Al_3(Zr,Er) precipitates demonstrate a high coarsening resistance [24,25] and improve the strength and recrystallization behavior [26–28]. The effect of Y with Zr in the structure and properties has not been investigated much [29]. Last year's investigations demonstrate the complex effect of Y and Er in Al alloys [30–39]. Yttrium or erbium with copper in Al provide the eutectic Al_8Cu_4Y(Er) phase formation [30–35]. The alloys with an atomic ratio Cu/Y(Er) equal to 4 have a narrow solidification interval with a high melting point [30–37]. In this case, the first role of the Y and Er is the eutectic forming elements. The Al_3(Zr,Y) or Al_3(Zr,Er) precipitates nucleate in a high-temperature homogenization treatment for Al-Cu-Y- and Al-Cu-Er-based alloys and improve the room- and high-temperature strength and recrystallization behavior [32–39]. This is the second role of Y and Er precipitates forming elements. Based on these two principles, novel heat-resistant cast and wrought Al alloys were developed [38,39]. Trace additives of Er or Y in Al–Zn–Mg–Cubased alloys affect the aging strengthening and corrosion resistance [40–45]. As a result, two basic principles should be taken into consideration to develop novel heat-resistant Al-Zn-Mg-Cu-based alloys with improved casting properties: 1—mass ratio of Zn/Mg = 1, and 2—atomic ratio of Cu/Y(Er) = 4. Based on these theses, the effect of yttrium and erbium in the phase composition, casting properties, room- and high-temperature mechanical properties of the Al–4.5Zn–4.5Mg–2.5Cu–0.2Zr alloy was investigated [46]. Additional alloying with Mn decreases the aging effect due to the formation of complex Mn-containing phases of a solidification origin [47]. A very high content in the alloying elements provides low deformation behavior. The main conclusion from a previous study is that the content of the Zn and Mg should be decreased and the Mn removed to improve the plasticity. The aim of the present investigation is to determine the effect of Y or Er alloying on the phase content, tensile properties and heat resistance of the Al–3Zn–3Mg–3Cu–0.2Zr alloy with Fe and Si impurities to develop novel cast and wrought alloys. The novel alloys should combine the high casting properties and strength at room and elevated temperatures.

2. Materials and Methods

2.1. Alloy Preparation

The Al3Zn3Mg3Cu, Al3Zn3Mg3CuY and Al3Zn3Mg3CuEr alloys (Table 1) were melted from pure Al (99.7%), Zn (99.7%), Mg (99.5%), Cu (99.5%) and Al-10Y, Al-10Er, Al-5Zr and Al-5Ti-1B master alloys in the resistance furnace. The melting and pouring temperatures were 800–810 °C. Pure copper and master alloys, rather than pure Zn and Mg, were introduced into the Al melt separately at 800–810 °C. Casting was carried out into a copper water-cooling mold (CM) and steel mold (SM). The ingot dimensions were 120 mm × 40 mm × 20 mm for a CM. The ingots from a copper water-cooling mold were used for rolling. The cylinders from SM with diameter of 24 mm and length of 290 mm were used for tensile test sample of cast alloys. The hot tearing of the alloys was determined via hot cracking index (HCI) using "pencil probe" [5,14].

Table 1. The chemical composition of the investigated alloys in wt.%.

Alloy	Al	Zn	Mg	Cu	Zr	Ti	Fe and Si	Y or Er
Al3Zn3Mg3Cu	bal.	2.8	2.7	3.0	0.2	0.1	0.3	-
Al3Zn3Mg3CuY	bal.	3.1	2.9	2.9	0.2	0.1	0.3	0.6
Al3Zn3Mg3CuEr	bal.	2.9	2.8	3.0	0.2	0.1	0.3	1.4

2.2. Microstructure and Phase Composition Analyses

The grain structure of the ingots and rolled sheets was analyzed with optical microscope (OM) Zeiss (Carl Zeiss, Oberkochen, Germany) and electron backscattered diffraction (EBSD) detector in scanning electron microscope (SEM) TESCAN VEGA 3LMH (Tescan, Brno, Czech Republic). OM was applied to grain structure analysis under polarized light. Microstructure and phase composition of the alloy were investigated in detail using SEM

and transmission electron microscope (TEM) JEOL—2100 EX (Jeol Ltd., Tokyo, Japan). SEM images were scanned in back-scattered electron (BSE) detector at ×3000 magnification at voltage of 20 kV. Phase identification in SEM was obtained using the electron diffraction X-ray (EDX) detector X-max 80. Additional phase analysis was performed using X-ray diffraction (XRD) with Cu-Kα radiation on a Bruker D8 Advance diffractometer (Bruker, Billerica, MA, USA). The XRD scanning was applied with $2\theta = 0.05^{\circ}$ step and dwell time of 5 s in a range of $2\theta = 20–90^{\circ}$.

2.3. Preparation of the Specimens for Microstructure Investigation

Specimens for OM and SEM investigation were mechanically ground and polished. Struers Labopol equipment was used for mechanical grinding and polishing. Grinding disk sheets with numbers of #800, #1200, #2000 and #4000 and OP-S suspension were used for specimen preparation. The grain structure for OM was electrochemically etched (15–25 V, 0–5 °C) using Barker's reagent (46 mL of HBF_4, 7 g of HBO_3 and 970 mL of H_2O). The average grain size value was measured using the random secant method in three images. The specimens for the TEM were prepared using the A2 electrolyte on Struers Tenupol-5 equipment. The TEM specimens were mechanically thinned to a 0.25 mm thickness before electrochemical procedure. The XRD investigation was conducted using alloy powder prepared through mechanical grinding.

2.4. Heat Treatment and Rolling Processing

The solidus and phase transformation temperatures of the alloys were determined via a Labsys Setaram differential scanning calorimeter (SETARAM Instrumentation, Caluire, France) (DSC). The solution treatment at 480–520 °C for 3 and 6 h was carried out in the resistant furnace with accuracy about 1 °C. The aging after solution treatment and water quenching was carried out at 120–250 °C in the resistant furnace with accuracy about 3 °C. The ingot after solution treatment at 480–520 °C and water quenching was hot rolled at 440 °C (Al3Zn3Mg3Cu) and 500 °C (Al3Zn3Mg3CuY and Al3Zn3Mg3CuEr) from thickness of 20 mm. The Al3Zn3Mg3Cu alloy ingot was rolled at 440 °C for 2 mm and at room temperature to 1 mm thickness sheet. The Al3Zn3Mg3CuY and Al3Zn3Mg3CuEr alloy ingots were rolled at 500 °C for 5 mm and at room temperature to 1 mm thickness sheets. Samples from rolled sheets were annealed at 150–450 °C for different times to investigate the grain structure, hardness and tensile properties evaluations. The rolled sheets were recrystallized at 480–520 °C for 15 min, water quenched and aged at 120–250 °C to determine the tensile properties.

2.5. Thermodynamic Calculations

Thermodynamic computations of the multicomponent phase equilibrium and non-equilibrium solidification (Sheil model) were carried out in the Thermo-Calc software in the TTAl5 database.

2.6. Mechanical Properties Measurements and Calculations

The Vickers method under 5 kg load was used for hardness measurements. The tensile samples were stretched on a Zwick/Roell Z250 Allround (Zwick/Roell, Kennesaw, GA, USA) test machine with an extensometer. The tensile samples with gage diameter of 6 mm and gage length of 42 mm were cut out from heat-treated ingots obtained in the steel mold. The tensile samples with gage width of 6 mm and gage length of 22 mm were cut out from 1 mm thickness sheets. Minimum 3 samples were tested per state, and average value was calculated. The rupture stress was determined on an Instron Creep M3 (Instron, Grove City, PA, USA) test machine.

3. Results and Discussion

3.1. Thermodynamic Calculation of the Phase Composition

Figure 1 illustrates the calculated phase equilibria in the Al–3Zn–3Mg–3Cu–0.1Ti–0.15Si–0.15Fe–(0–0.4)Zr system and non-equilibrium cooling curve of the Al3Zn3Mg3Cu alloy. The increase in Zr content in the Al–3Zn–3Mg–3Cu–0.1Ti–0.15Si–0.15Fe alloy provides an increase in the liquidus temperature from about 680 °C in the alloy without Zr to 800 °C in the alloy with 0.27%Zr (Figure 1a). The melting of the Zn and Mg content alloy should be proceeded at temperatures lower than 800 °C to avoid the losses of these elements. In this case, the maximum content of Zr should be 0.2%. The solidification of the Al3Zn3Mg3Cu alloy starts from Al_3(Zr,Ti) phase nucleation due to the calculated cooling curve (Figure 1b). The Sheil model includes the assumption that the distributive and equalizing diffusion in a liquid was completely processed. However the formation of the Al_3(Zr,Ti) usually suppresses, and the clusters of the Al_3(Zr,Ti) have a role as a substrate for primary aluminum solid solution (Al). Al_3Fe, Mg_2Si, Al_7Cu_2Fe, S(Al_2CuMg), T (Al,Zn,Mg,Cu) and $MgZn_2$ phases solidify during non-equilibrium solidification (Figure 1b).

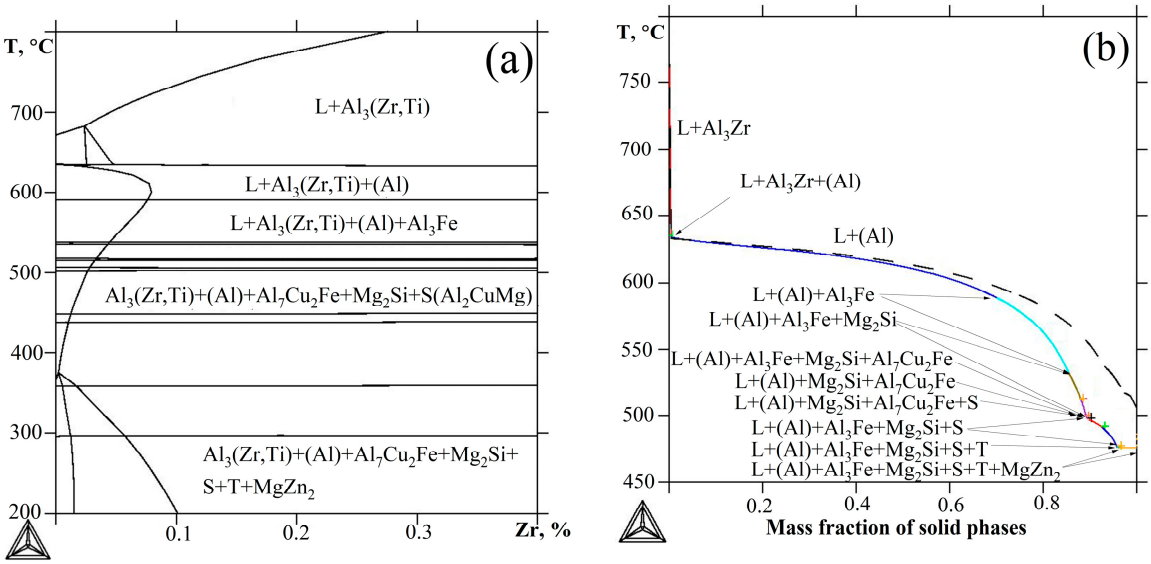

Figure 1. Calculated (**a**) polythermal section Al–3Zn–3Mg–3Cu–0.1Ti–0.15Si–0.15Fe– (0-0.4)Zr and (**b**) non-equilibrium cooling curve of the Al3Zn3Mg3Cu alloy (dash line—equilibrium cooling curve).

The non-equilibrium cooling curve should be used to calculate the effective solidification range (ESR) and the HCI of the alloys [14]. The ESR of the Al–Zn–Mg–Cu-based alloy should be calculated as a difference between temperature in the 65% of solid phase formation and non-equilibrium solidus [14]. The linear empirical equation was used to calculate the HCI using the calculated value of the ESR (Table 2). The HCI = 14 mm is suitable for the Al-Si-Cu-Mg-based alloys with good casting properties [48]. Additional alloying of the Al3Zn3Mg3Cu alloy with Y or Er should improve the casting properties due to the eutectic fraction increasing. The experimental HCI of the Al3Zn3Mg3Cu is 14–16 mm and 14 mm for the Al3Zn3Mg3CuY and Al3Zn3Mg3CuEr alloys.

Table 2. Calculated critical temperatures, ESR and HCI of the Al3Zn3Mg3Cu alloy.

T_L, °C	T_S, °C	$T_{65\%}$, °C	T_{NS}, °C	ESR, °C	HCI_c, mm
761	505	595	475	120	14

3.2. As-Cast Microstructure and Phase Composition

The investigated alloys were poured into SM and CM. The cooling rate in the steel and copper molds was different, which may affect the microstructure. Figures 2 and 3

demonstrate the grain and dendritic cell structure of the as-cast alloys. Differences in the cooling rate do not affect the grain structure of the alloys (compare a–c and d–e images in Figure 2). The average grain size of the Al3Zn3Mg3Cu alloy is 100 ± 15 µm (Figure 2a,d). Yttrium and erbium may substitute the Zr or Ti atom in the Al_3(Zr,Ti) phase clusters and increase the volume fraction of the substrates for primary (Al). As a result, a slightly fine grain structure with a size of 80 ± 10 µm was obtained in the ingots of the Al3Zn3Mg3CuY alloy (Figure 2b,e). Erbium provides a significantly higher refining effect, as indicated in the literature [38–43]. An average grain size of 45 ± 10 µm was obtained in the Al3Zn3Mg3CuEr ingots (Figure 2c,f).

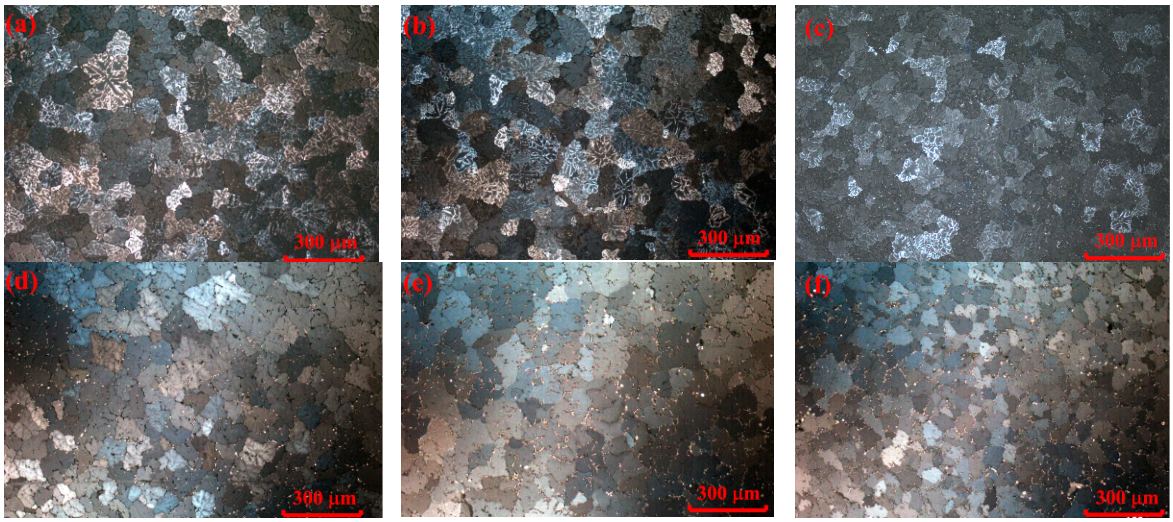

Figure 2. (**a**–**c**) As-cast grain structure of the (**a**,**d**) Al3Zn3Mg3Cu, (**b**,**e**) Al3Zn3Mg3CuY and (**c**,**f**) Al3Zn3Mg3CuEr alloys poured into (**a**–**c**) CM and (**d**,**e**) SM.

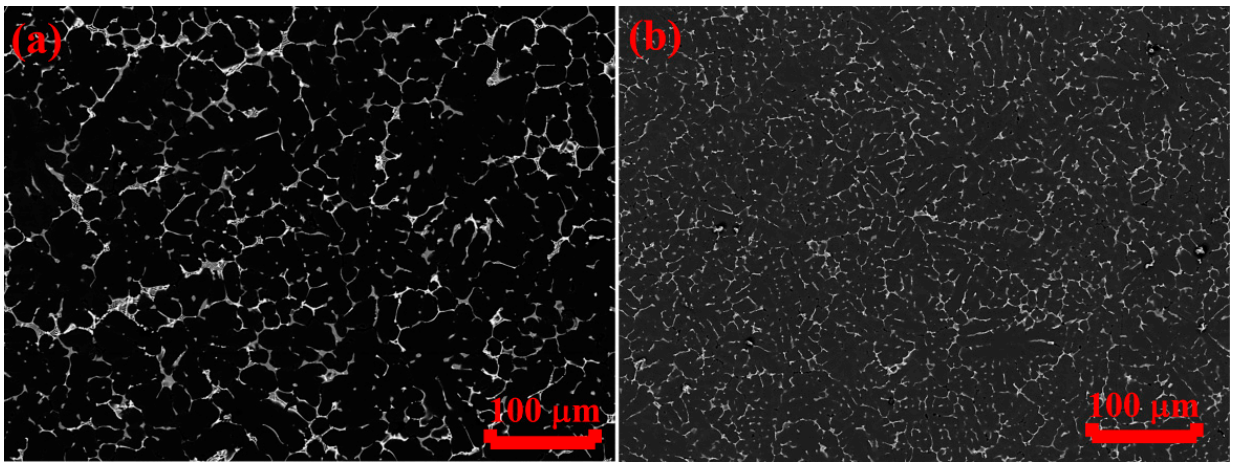

Figure 3. As-cast microstructure of the Al3Zn3Mg3CuY alloy poured into (**a**) SM and (**b**) CM.

The cooling rate in the copper mold is higher than in the steel one, which provides a finer dendritic cell structure in the ingots poured into the coper mold (Figure 3). The size of the secondary dendritic arm spacing (SDAS) in the SM and CM ingots is 22 ± 4 µm and 12 ± 3 µm, respectively (Figure 3). This difference in the SDAS size is not significant for mechanical properties, as demonstrated by the authors in [49].

The as-cast microstructure and XRD patterns of the Al3Zn3Mg3Cu, Al3Zn3Mg3CuY and Al3Zn3Mg3CuEr alloys are presented in Figure 4. Three phase particles are presented in the microstructure of the Al3Zn3Mg3Cu alloy: Zn-, Cu- and Mg-rich particles, Mg- and Si-rich particles and Cu- and Fe-rich particles correspond to T, Mg_2Si and Al_7Cu_2Fe

phases (Figure 4a). These results are in good agreement with calculation (Figure 1) and XRD (Figure 4d) data. The main peaks at angles of about 27, 32, 35 and 41° are marked as S phase (XRD card no. 03-065-2504). The peaks at 37 and 40.5° correspond to the T phase (XRD card no. 00-043-1442 (Q)). The main peaks from (Al) cover some peaks from S and T phases. A very low fraction of S phase particles was also identified in the microstructure. Point analyses demonstrate the presence of 2–4%Zn in these particles. Zn atoms may substitute Al in the phase. Al_8Cu_4Y and A_8Cu_4Er phases formed in the Al3Zn3Mg3CuY and Al3Zn3Mg3CuEr alloys, respectively, in addition to the T and Mg_2Si phases (Figure 4b–d). The main two peaks at 41 and 41.5° are indicated for Al_8Cu_4Y and A_8Cu_4Er phases (Figure 4d, XRD card no. 01-070-9419 and 00-033-0006 (I), respectively). Fe impurity dissolved in the Al_8Cu_4Y and A_8Cu_4Er phases (see the distribution of the alloying elements between phases) at 1–2% content. The same results were obtained in an earlier investigation [38]. Separate particles of the $(Al,Cu)_{11}Y_3$ (XRD card no. 01-070-9423) and Al_3Er (XRD card no. 03-065-9825) with dissolved Zn were also identified in the Al3Zn3Mg3CuY and Al3Zn3Mg3CuEr alloys, respectively. Zirconium completely dissolved in the (Al) in all investigated alloys, without coarse particle formation. Yttrium and erbium content in the (Al) was 0.2 and 0.3%, respectively.

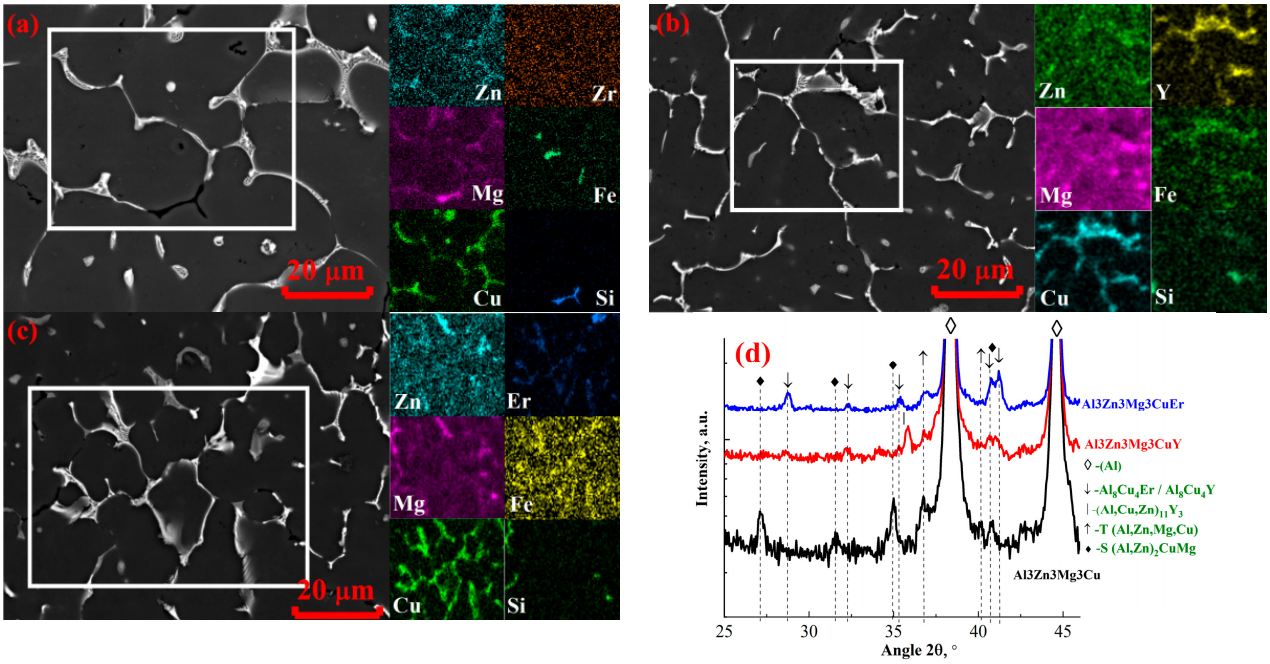

Figure 4. As-cast microstructure of the (**a**) Al3Zn3Mg3Cu, (**b**) Al3Zn3Mg3CuY and (**c**) Al3Zn3Mg3CuEr alloys and (**d**) XRD patterns (distribution of alloying elements into white rectangle in (**a**–**c**)).

3.3. Evaluation of the Microstructure under Solution Treatment

The DSC curves of the investigated alloys are presented in Figure 5. Three melting peaks of the T, Al_7Cu_2Fe and Mg_2Si at temperatures of 493, 525 and 540 °C were identified on the heating DSC curves of the investigated alloys. The Y- and Er-containing phases in the Al3Zn3Mg3CuY and Al3Zn3Mg3CuEr alloys melted in a temperature range of 540–580 °C. The small peak at 477 °C was found in the Al3Zn3Mg3CuEr alloy, which corresponded to the $MgZn_2$ phase in accordance with the calculation (Figure 1b). The investigated alloys were solution-treated at 480 °C for 3 h. The non-equilibrium fraction of T, S and $MgZn_2$ phases dissolved during solution treatment. These phases dissolved completely in the Al3Zn3Mg3CuY and Al3Zn3Mg3CuEr alloys. The solidus temperature of the Al3Zn3Mg3CuY and Al3Zn3Mg3CuEr alloys increased to 533 °C (Figure 5b).

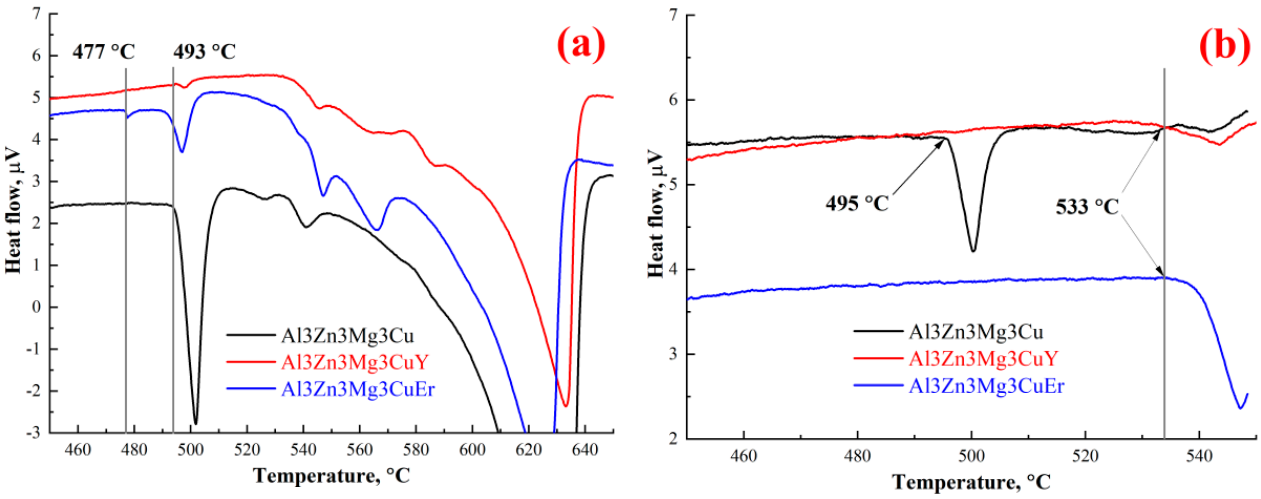

Figure 5. DSC curves of the (**a**) as-cast and (**b**) solution treated at 480 °C for 3 h alloys.

Figure 6 demonstrates the microstructure changes. The T phase transforms to S phase and spheroidizes in the Al3Zn3Mg3Cu alloy (Figure 6a). These results are in good agreement with the calculations. The S, Mg_2Si, Al_7Cu_2Fe and Al_3(Zr,Ti) should be in equilibrium with (Al) in accordance with the calculation (Table 3). The Al_3(Zr,Ti) phase must nucleate from the supersaturated (Al) during solution treatment. The Y- and Er-containing phases in the Al3Zn3Mg3CuY and Al3Zn3Mg3CuEr alloys (Figure 6b,c) do not significantly change the morphology compared to the as-cast state (Figure 4b,c). This fact confirms a high thermal stability of Y- and Er-containing phases.

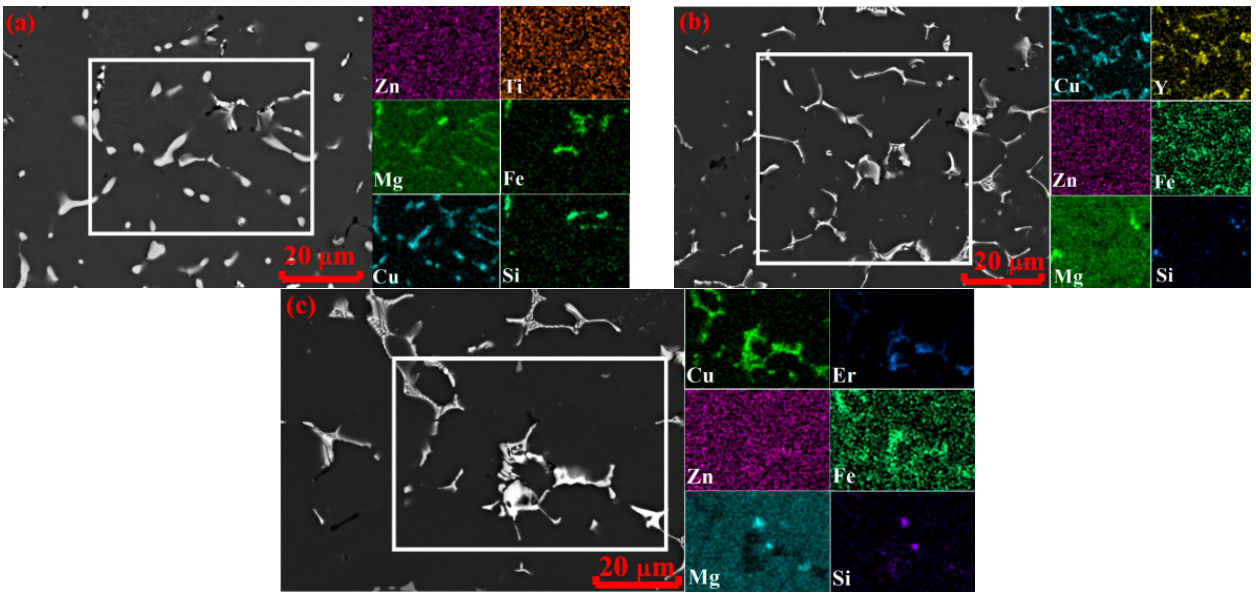

Figure 6. Microstructure of the of the (**a**) Al3Zn3Mg3Cu, (**b**) Al3Zn3Mg3CuY and (**c**) Al3Zn3Mg3CuEr alloys after solution treatment at 480 °C for 3 h.

Table 3. Calculated mass fraction of phases and composition of (Al) at 480 °C.

(Al)	S	Al_7Cu_2Fe	Mg_2Si	Al_3(ZrTi)
bal. (3.1Zn-2.6Mg-2.1Cu)	1.5	1	0.37	0.4

The second step of the solution treatment at 520 °C for 6 h was applied to the Al3Zn3Mg3CuY and Al3Zn3Mg3CuEr alloys. The Y- and Er-containing phase particles fragmentized and sheroidized (Figure 7). The microstructure with more compact particles of the solidification origin should provide better plasticity. The experimentally measured composition of the (Al) is presented in Table 4. The Mg content in the (Al) of the Al3Zn3Mg3Cu alloy is lower than in the Y- and Er-containing alloys due to the presence of the S phase. However, the Cu content in the Al3Zn3Mg3CuY and Al3Zn3Mg3CuEr alloys is lower than in the Al3Zn3Mg3Cu alloy due to the presence of Y- and Er-containing phases. In addition, the Y and Er solute atoms in the (Al) during solidification should provide a higher fraction of the precipitates after solution treatment in the Al3Zn3Mg3CuY and Al3Zn3Mg3CuEr alloys.

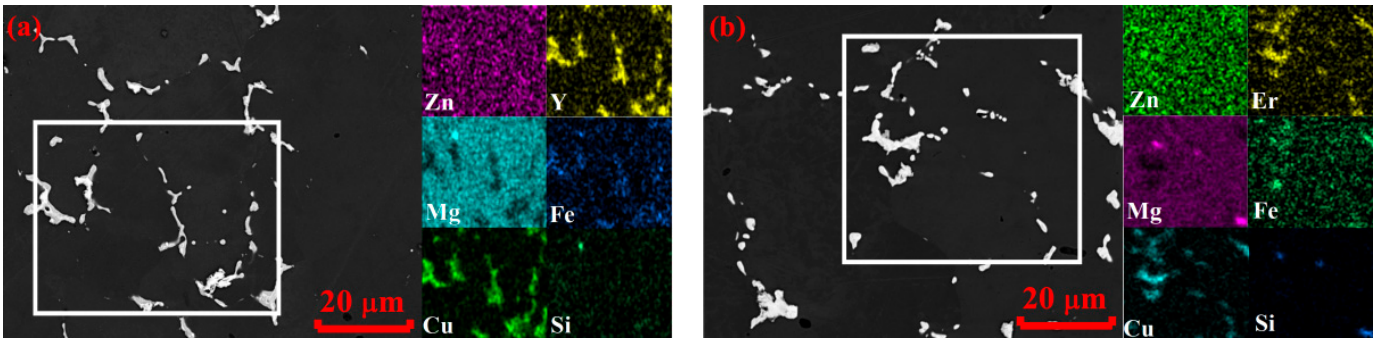

Figure 7. Microstructure of the (**a**) Al3Zn3Mg3CuY and (**b**) Al3Zn3Mg3CuEr alloys after solution treatment at 480 °C for 3 h + 520 °C for 6 h.

Table 4. Composition of the Al solid solution in mass.% (EDX SEM).

Alloy	As-Cast State			480 °C, 3 h			480 °C, 3 h + 520 °C, 6 h		
	Zn	Mg	Cu	Zn	Mg	Cu	Zn	Mg	Cu
Al3Zn3Mg3Cu	2.7	2.0	0.6	3.2	2.5	1.6	-	-	-
Al3Zn3Mg3CuY	2.2	2.2	1.0	3.0	3.0	1.3	3.1	3.1	1.3
Al3Zn3Mg3CuEr	2.2	1.9	1.0	3.0	3.0	1.2	3.0	3.0	1.2

3.4. Hardening under Aging Treatment and Mechanical Properties

The metastable $MgZn_2$(1.4–3 mass.%), S (0.8–1.3 mass.%) and T (5.7–6.2 mass.%) phases should provide strengthening during aging at 120–210 °C for the Al3Zn3Mg3Cu alloy in accordance with the measured composition of (Al) (Table 4) and calculations. The same calculation for the Al3Zn3Mg3CuY and Al3Zn3Mg3CuEr alloys shows that the T (8.7–9.9 mass.%) phase should be nucleated during aging. Figure 8 illustrates the HV curves at different aging temperatures of the alloys quenched at 480 °C and 520 °C (for the Al3Zn3Mg3CuY and Al3Zn3Mg3CuEr alloys). The highest strengthening was achieved in the Al3Zn3Mg3Cu alloy due to the formation of $MgZn_2$ and S phases. Slightly higher strengthening was achieved after a two-step solution treatment. The Er- or Y-containing precipitates that formed during the solution treatment may affect the aging process [40–45]. The size and distribution of the precipitates after a one- and two-step solution treatment are different. A detailed investigation of the precipitation strengthening will be presented in a future paper.

The hardness of 120–140 HV was achieved after 40–50 h of annealing at 120–150 °C in all investigated alloys. Slightly lower strengthening was achieved after aging at 180–210 °C. The aging temperature of the heat-resistant alloys should cover the operating temperatures. In this case, aging at 210 °C for 3 h was applied for investigated alloys before tensile tests at room and elevated temperatures.

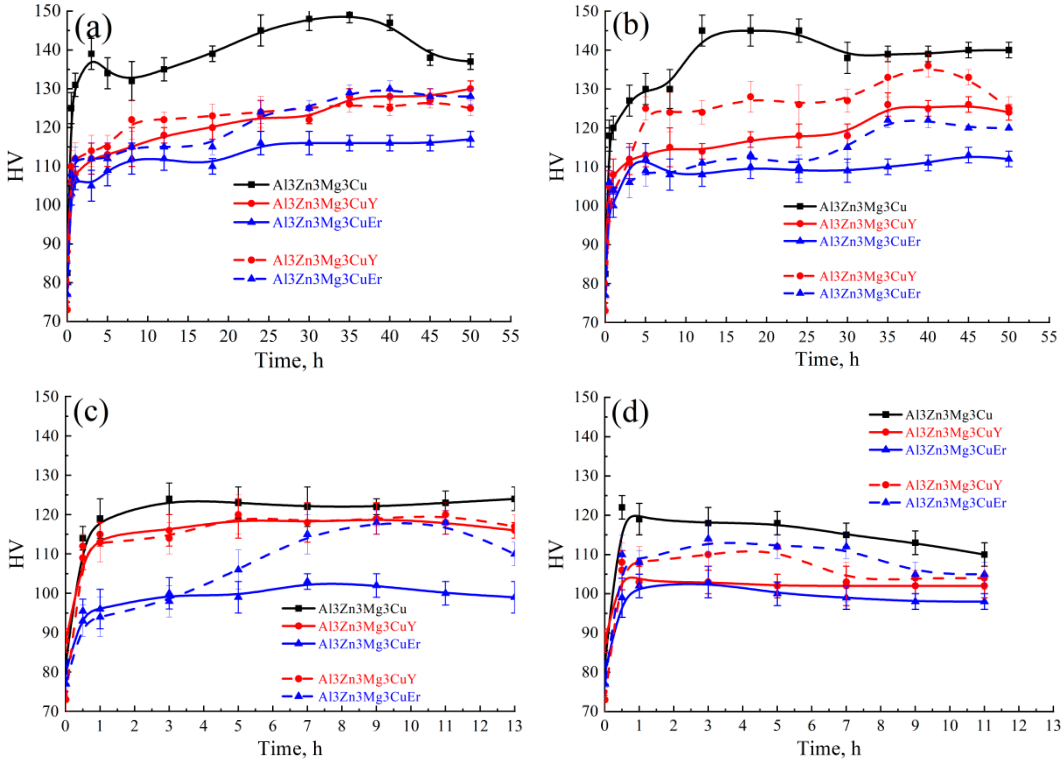

Figure 8. HV curves at different aging temperatures (**a**) 120 °C, (**b**) 150 °C, (**c**) 180 °C and (**d**) 210 °C (solid lines—quenched at 480 °C, dash lines—quenched at 520 °C).

The tensile test results after tension at room and elevated temperatures are presented in Table 5. The Al3Zn3Mg3Cu alloy was solution-treated at 480 °C for 3 h and water quenched. A two-step solution treatment with water quenching was applied for the Al3Zn3Mg3CuY and Al3Zn3Mg3CuEr alloys: 480 °C for 3 h and 520 °C for 6 h. The investigated alloys demonstrate a good YS of 270–290 MPa at room temperature. The two-step solution treatment provides a higher elongation of 2–3% for the Al3Zn3Mg3CuY and Al3Zn3Mg3CuEr alloys. The YS decreased insignificantly from 270–290 MPa to 225–260 MPa after tension at 200 °C. The commercial cast 771.0 (7Zn–0.9Mg–0.13Cr) alloy had a substantially lower YS = 185 MPa and the same elongation of 3% after aging at 205 °C for 6 h [6].

Table 5. Tensile properties of the alloys aged at 210 °C for 3 h at different temperatures.

Alloy	YS, MPa	UTS, MPa	El., %
	20 °C		
Al3Zn3Mg3Cu	290 ± 10	340 ± 20	1.4 ± 0.4
Al3Zn3Mg3CuY	280 ± 8	340 ± 20	3 ± 1
Al3Zn3Mg3CuEr	270 ± 4	330 ± 10	2.0 ± 0.5
	200 °C		
Al3Zn3Mg3Cu	260 ± 8	270 ± 6	3.0 ± 0.5
Al3Zn3Mg3CuY	230 ± 6	250 ± 5	5.2 ± 0.2
Al3Zn3Mg3CuEr	225 ± 4	237 ± 6	3.5 ± 0.6

3.5. Microstructure and Hardness Evaluation after Rolling and Annealing

The high content of the alloying elements and high fraction of the solidification origin phases may decrease the manufacturability during rolling. An increase in the rolling temperature provides rolled sheets without cracks and defects. The higher solidus temperature of the Al3Zn3Mg3CuY and Al3Zn3Mg3CuEr alloys after a two-step solution treatment may possibly increase the rolling temperature. Al3Zn3Mg3CuY and Al3Zn3Mg3CuEr alloy

sheets were obtained with a higher fraction of cold deformation than the Al3Zn3Mg3Cu alloy sheet. As a result, higher hardness was achieved in the Y- and Er-containing alloys (Figure 9). A higher deformation strengthening provides a faster softening during annealing of the rolled sheets at temperatures lower than 250 °C. Deformed grain structure is maintained up to 300 °C. The recrystallized grains were found after 1 h of annealing at 350 °C (Figure 10a–c). A significantly finer grain structure was achieved in the Al3Zn3Mg3CuY and Al3Zn3Mg3CuEr alloys due to a higher content of rare earth elements, the precipitates of which suppress recrystallization.

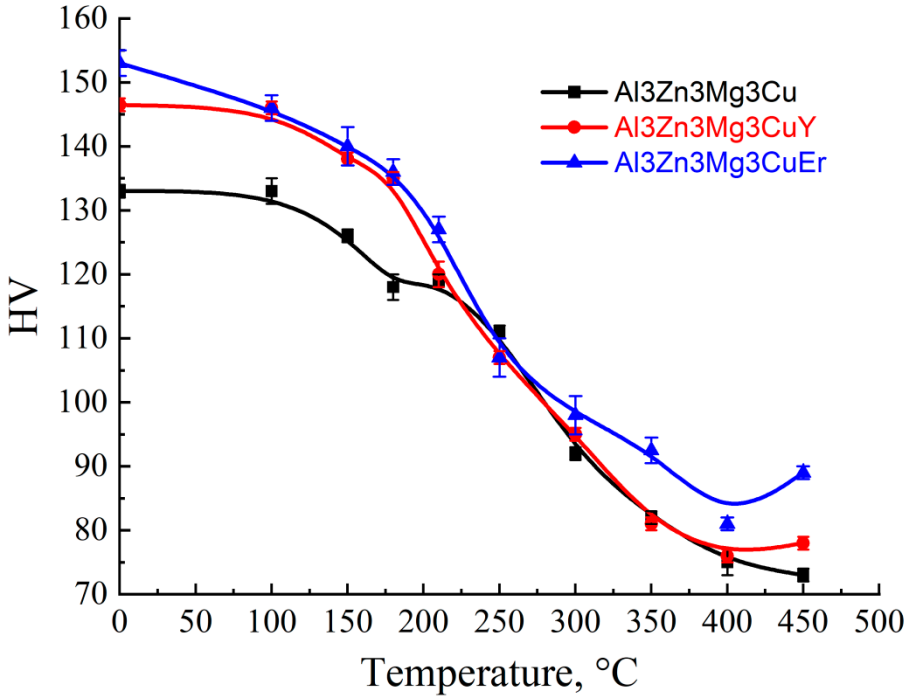

Figure 9. HV–temperature curves after 1 h of annealing of the alloy sheets.

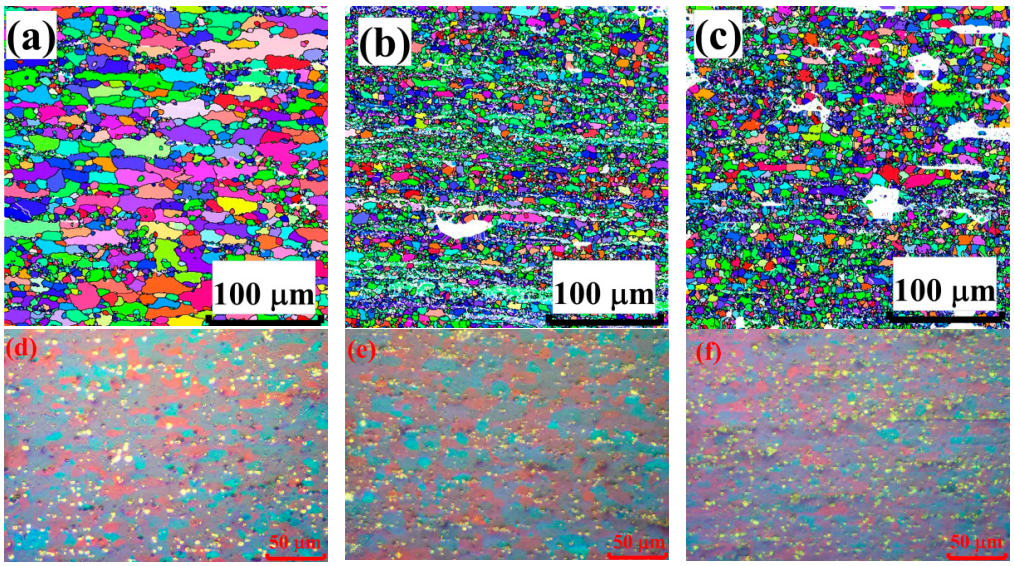

Figure 10. Grain structure of the (**a**,**d**) Al3Zn3Mg3Cu, (**b**,**e**) Al3Zn3Mg3CuY and (**c**,**f**) Al3Zn3Mg3CuEr alloys after 1 h of annealing at (**a**–**c**) 350 °C (EBSD) and after 15 min of annealing at (**d**) 480 °C (OM) and (**e**,**f**) 520 °C (OM).

The Al3Zn3Mg3Cu alloy was recrystallized at 480 °C for 15 min and water quenched. The Al3Zn3Mg3CuY and Al3Zn3Mg3CuEr alloys were recrystallized at 520 °C for 15 min

and water quenched. The uniform recrystallized grain structure with a size of 8–10 μm was formed in the investigated alloys (Figure 10d–f).

The aging strengthening of the rolled sheet (Figure 11) is similar to the aging of the cast, solution-treated and water-quenched alloys (Figure 7). The tensile test results of the aged alloys sheets at different temperatures are presented in Table 6. A better combination of the YS = 291–345 MPa and elongation (11–14.8%) was achieved in the Al3Zn3Mg3CuY and Al3Zn3Mg3CuEr alloys in comparison to the Al3Zn3Mg3Cu alloy with YS = 245–340 MPa and El. = 6.8–12.5%.

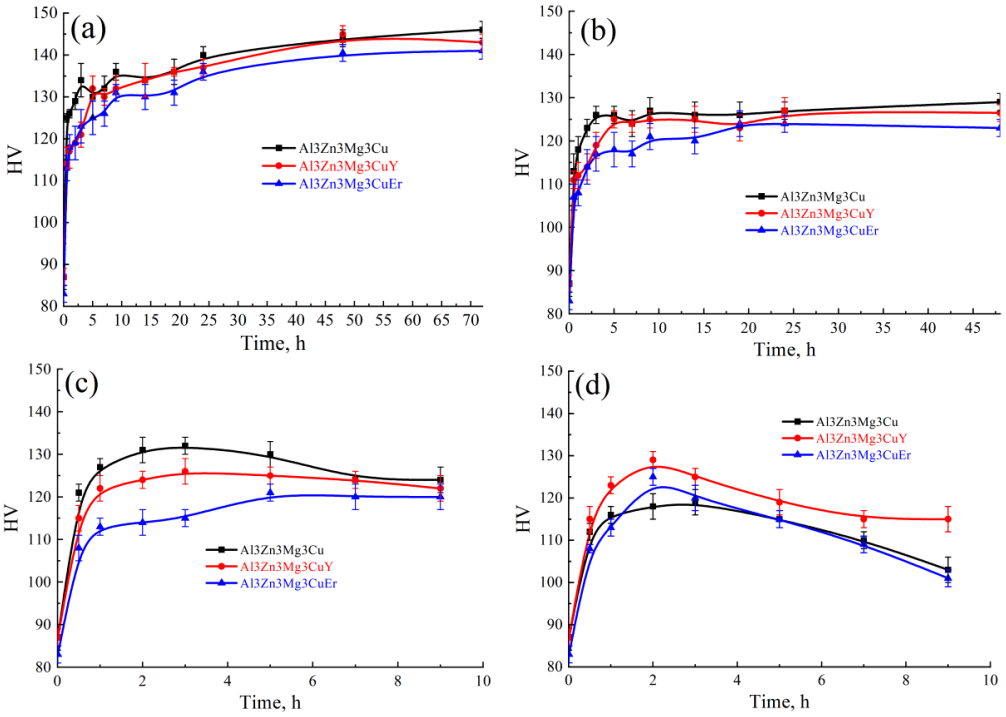

Figure 11. HV curves at different aging temperatures (**a**) 120 °C, (**b**) 150 °C, (**c**) 180 °C and (**d**) 210 °C (Al3Zn3Mg3Cu alloy quenched at 480 °C after 15 min, Al3Zn3Mg3CuY and Al3Zn3Mg3CuEr alloys quenched at 520 °C after 15 min).

Table 6. Tensile properties of the rolled, quenched and aged alloy sheets.

State	YS, MPa	UTS, MPa	El., %
Al3Zn3Mg3Cu			
As rolled	407 ± 2	440 ± 1	4.0 ± 0.4
480 °C for 15 min/120 °C for 48 h	340 ± 10	440 ± 10	8.0 ± 1.0
480 °C for 15 min/150 °C for 32 h	290 ± 7	435 ± 15	9 ± 3
480 °C for 15 min/180 °C for 5 h	285 ± 5	425 ± 5	12.5 ± 0.5
480 °C for 15 min/210 °C for 2 h	245 ± 10	370 ± 5	6.8 ± 0.3
Al3Zn3Mg3CuY			
As rolled	455 ± 8	477 ± 3	2 ± 1.5
520 °C for 15 min/120 °C for 48 h	345 ± 2	471 ± 2	12.8 ± 1.2
520 °C for 15 min/150 °C for 32 h	315 ± 1	460 ± 1	13.6 ± 0.2
520 °C for 15 min/180 °C for 5 h	291 ± 2	449 ± 1	14.8 ± 1.5
520 °C for 15 min/210 °C for 2 h	316 ± 1	430 ± 1	10.3 ± 1.5
Al3Zn3Mg3CuEr			
As rolled	450 ± 2	474 ± 3	3.7 ± 0.5
520 °C for 15 min/120 °C for 48 h	334 ± 1	446 ± 1	14.8 ± 0.1
520 °C for 15 min/150 °C for 32 h	300 ± 2	434 ± 3	12.5 ± 2
520 °C for 15 min/180 °C for 5 h	295 ± 13	445 ± 5	14.8 ± 0.5
520 °C for 15 min/210 °C for 2 h	303 ± 1	413 ± 1	11 ± 2

4. Conclusions

The microstructure, phase transformation and mechanical properties of the novel cast and wrought Al–3Zn–3Mg–3Cu–0.2Zr–Y(Er) alloys were investigated. Thermodynamic calculation was calculated with optical and scanning electron microscopy, and the X-ray diffraction methods were used for phase identification.

The Y and Er addition in the Al3Zn3Mg3Cu alloy increased the solidus temperature from 493 to 533 °C. A two-step solution treatment (480 °C, 3 h + 520 °C, 6 h) with higher temperature in the second step provided the microstructure with better elongation and made it possible to increase the temperature of the hot rolling. The YS of the cast, solution-treated, water-quenched and aged alloys decreased insignificantly from 270–290 MPa at room temperature to 225–260 MPa after tension at 200 °C. A significantly finer-grain structure was achieved in the Al3Zn3Mg3CuY and Al3Zn3Mg3CuEr alloys after rolling and annealing due to a higher content of the rare earth elements precipitating to suppress recrystallization. A better combination of the YS=291-345 MPa and elongation (11–14.8%) was achieved in the Al3Zn3Mg3CuY and Al3Zn3Mg3CuEr alloys after solution treatment, rolling (hot and cold), recrystallization annealing (520 °C, 15 min), water quenching and aging (120–210 °C) in comparison with the Al3Zn3Mg3Cu alloy with YS = 245–340 MPa and El. = 6.8–12.5%.

Author Contributions: Conceptualization, A.V.P.; methodology, M.V.G. and L.E.G.; formal analysis, M.G.K. and A.V.P.; investigation, R.Y.B. and A.V.P.; data curation, M.G.K., R.Y.B.; writing—original draft preparation, A.V.P.; writing—review and editing, A.V.P.; visualization, M.V.G. and A.V.P.; supervision, A.V.P.; funding acquisition, M.G.K. All authors have read and agreed to the published version of the manuscript.

Funding: The work was supported by the Russian Science Foundation (Project No. 22-79-10142), https://rscf.ru/project/22-79-10142/, accessed on 4 May 2023.

Conflicts of Interest: The authors declare no conflict of interest.

References

1. Gerchikova, N.S.; Fridlyander, I.N.; Zaitseva, N.I.; Kirkina, N.N. Change in the structure and properties of Al-Zn-Mg alloys. *Met. Sci. Heat Treat.* **1972**, *14*, 233–236. [CrossRef]
2. Zolotorevsky, V.S. Microstructure and Mechanical Properties of Cast Aluminum Alloys. Ph.D. Thesis, MISIS, Moscow, Russia, 1979. (In Russian)
3. Zou, Y.; Wu, X.; Tang, S.; Zhu, Q.; Song, H.; Guo, M.; Cao, L. Investigation on microstructure and mechanical properties of Al-Zn-Mg-Cu alloys with various Zn/Mg ratios. *J. Mater. Sci. Technol.* **2021**, *85*, 106–117. [CrossRef]
4. Novikov, I.I. *Hot-Shortness of Non-Ferrous Metals and Alloys*; Nauka: Moscow, Russia, 1966. (In Russian)
5. Pan, Y.; Zhang, D.; Liu, H.; Zhuang, L.; Zhang, J. Precipitation hardening and intergranular corrosion behavior of novel Al–Mg–Zn(-Cu) alloys. *J. Alloys Compd.* **2021**, *853*, 157199. [CrossRef]
6. ASM International Handbook Committee. *ASM Handbook Volume 2: Properties and Selection—Nonferrous Alloys and Special-Purpose Materials*; ASM: Almere, The Netherlands, 2001; ISBN 0871700077.
7. Belov, N.A.; Alabin, A.N.; Eskin, D.G.; Istomin-Kastrovskii, V.V. Optimization of hardening of Al–Zr–Sc cast alloys. *J. Mater. Sci.* **2006**, *41*, 5890–5899. [CrossRef]
8. Shurkin, P.K.; Akopyan, T.K.; Galkin, S.P.; Aleshchenko, A.S. Effect of Radial Shear Rolling on the Structure and Mechanical Properties of a New-Generation High-Strength Aluminum Alloy Based on the Al-Zn-Mg-Ni-Fe System. *Met. Sci. Heat Treat.* **2019**, *60*, 764–769. [CrossRef]
9. Akopyan, T.K.; Belov, N.A.; Alabin, A.N.; Zlobin, G.S. Calculation-experimental study of the aging of casting high-strength Al-Zn-Mg-(Cu)-Ni-Fe aluminum alloys. *Russ. Metall.* **2014**, *2014*, 60–65. [CrossRef]
10. David, M.D.; Foley, R.D.; Griffin, J.A.; Monroe, C.A. Microstructural Characterization and Thermodynamic Simulation of Cast Al-Zn-Mg-Cu Alloys. *Int. J. Met.* **2016**, *10*, 2–20. [CrossRef]
11. Petrova, A.N.; Brodova, I.G.; Razorenov, S.V.; Shorokhov, E.V.; Akopyan, T.K. Mechanical Properties of the Al–Zn–Mg–Fe–Ni Alloy of Eutectic Type at Different Strain Rates. *Phys. Met. Metallogr.* **2019**, *120*, 1221–1227. [CrossRef]
12. Brodova, I.G.; Shirinkina, I.G.; Rasposienko, D.Y.; Akopyan, T.K. Structural Evolution in the Quenched Al–Zn–Mg–Fe–Ni Alloy during Severe Plastic Deformation and Annealing. *Phys. Met. Metallogr.* **2020**, *121*, 899–905. [CrossRef]
13. Zolotorevskii, V.S.; Pozdnyakov, A.V.; Churyumov, A.Y. Search for promising compositions for developing new multiphase casting alloys based on Al-Zn-Mg matrix using thermodynamic calculations and mathematic simulation. *Phys. Met. Metallogr.* **2014**, *115*, 286–294. [CrossRef]

14. Pozdniakov, A.V.; Zolotorevskiy, V.S.; Mamzurina, O.I. Determining hot cracking index of Al–Mg–Zn casting alloys calculated using effective solidification range. *Int. J. Cast Met. Res.* **2015**, *28*, 318–321. [CrossRef]
15. Guangyu, Y.; Shaojun, L.; Wanqi, J. Effects of minor Sc addition on the microstructures and mechanical properties of Al-Zn-Mg-Cu casting aluminum alloy. In *The Minerals, Metals & Materials Series*; Elsevier: Amsterdam, The Netherlands, 2016; pp. 463–467.
16. Nadella, R.; Eskin, D.; Katgerman, L. Effect of grain refining on defect formation in DC Cast Al-Zn-Mg-Cu alloy billet. In *Essential Readings in Light Metals*; Springer International Publishing: Cham, Switzerland, 2016; pp. 842–847.
17. Senkov, O.N.; Bhat, R.B.; Senkova, S.V.; Schloz, J.D. Microstructure and properties of cast ingots of Al-Zn-Mg-Cu alloys modified with Sc and Zr. *Metall. Mater. Trans. A* **2005**, *36*, 2115–2126. [CrossRef]
18. He, Y.; Zhang, X.; You, J. Effect of minor Sc and Zr on microstructure and mechanical properties of Al-Zn-Mg-Cu alloy. *Trans. Nonferrous Met. Soc. China* **2006**, *16*, 1228–1235. [CrossRef]
19. Srinivasan, S.; Desch, P.B.; Schwarz, R.B. Metastable phases in the Al3X (X = Ti, Zr, and Hf) intermetallic system. *Scr. Metall. Mater.* **1991**, *25*, 2513–2516. [CrossRef]
20. Knipling, K.E.; Dunand, D.C.; Seidman, D.N. Precipitation evolution in Al–Zr and Al–Zr–Ti alloys during isothermal aging at 375–425 °C. *Acta Mater.* **2008**, *56*, 114–127. [CrossRef]
21. Gao, H.; Feng, W.; Wang, Y.; Gu, J.; Zhang, Y.; Wang, J.; Sun, B. Structural and compositional evolution of Al3(Zr,Y) precipitates in Al-Zr-Y alloy. *Mater. Charact.* **2016**, *121*, 195–198. [CrossRef]
22. Knipling, K.E.; Dunand, D.C.; Seidman, D.N. Precipitation evolution in Al-Zr and Al-Zr-Ti alloys during aging at 450–600 °C. *Acta Mater.* **2008**, *56*, 1182–1195. [CrossRef]
23. Knipling, K.; Dunand, D. Creep resistance of cast and aged Al–0.1Zr and Al–0.1Zr–0.1Ti (at.%) alloys at 300–400 °C. *Scr. Mater.* **2008**, *59*, 387–390. [CrossRef]
24. Wen, S.P.; Gao, K.Y.; Li, Y.; Huang, H.; Nie, Z.R. Synergetic effect of Er and Zr on the precipitation hardening of Al–Er–Zr alloy. *Scr. Mater.* **2011**, *65*, 592–595. [CrossRef]
25. Li, H.; Bin, J.; Liu, J.; Gao, Z.; Lu, X. Precipitation evolution and coarsening resistance at 400 °C of Al microalloyed with Zr and Er. *Scr. Mater.* **2012**, *67*, 73–76. [CrossRef]
26. Wen, S.P.; Gao, K.Y.; Huang, H.; Wang, W.; Nie, Z.R. Precipitation evolution in Al-Er-Zr alloys during aging at elevated temperature. *J. Alloys Compd.* **2013**, *574*, 92–97. [CrossRef]
27. Gao, Z.; Li, H.; Lai, Y.; Ou, Y.; Li, D. Effects of minor Zr and Er on microstructure and mechanical properties of pure aluminum. *Mater. Sci. Eng. A* **2013**, *580*, 92–98. [CrossRef]
28. Li, H.; Gao, Z.; Yin, H.; Jiang, H.; Su, X.; Bin, J. Effects of Er and Zr additions on precipitation and recrystallization of pure aluminum. *Scr. Mater.* **2013**, *68*, 59–62. [CrossRef]
29. Huang, H.; Wen, S.P.; Gao, K.Y.; Wang, W.; Nie, Z.R. Age hardening behavior and corresponding microstructure of dilute Al-Er-Zr alloys. *Metall. Mater. Trans. A Phys. Metall. Mater. Sci.* **2013**, *44*, 2849–2856. [CrossRef]
30. Pozdniakov, A.V.; Barkov, R.Y. Microstructure and materials characterisation of the novel Al–Cu–Y alloy. *Mater. Sci. Technol.* **2018**, *34*, 1489–1496. [CrossRef]
31. Amer, S.M.; Barkov, R.Y.; Yakovtseva, O.A.; Pozdniakov, A.V. Comparative Analysis of Structure and Properties of Quasibinary Al–6.5Cu–2.3Y and Al–6Cu–4.05Er Alloys. *Phys. Met. Metallogr.* **2020**, *121*, 476–482. [CrossRef]
32. Pozdnyakov, A.V.; Barkov, R.Y.; Sarsenbaev, Z.; Amer, S.M.; Prosviryakov, A.S. Evolution of Microstructure and Mechanical Properties of a New Al–Cu–Er Wrought Alloy. *Phys. Met. Metallogr.* **2019**, *120*, 614–619. [CrossRef]
33. Pozdniakov, A.V.; Barkov, R.Y.Y.; Amer, S.M.; Levchenko, V.S.; Kotov, A.D.; Mikhaylovskaya, A.V. Microstructure, mechanical properties and superplasticity of the Al–Cu–Y–Zr alloy. *Mater. Sci. Eng. A* **2019**, *758*, 28–35. [CrossRef]
34. Amer, S.M.; Barkov, Y.R.; Yakovtseva, O.A.; Loginova, I.S.; Pozdniakov, A.V. Effect of Zr on microstructure and mechanical properties of the Al–Cu–Er alloy. *Mater. Sci. Technol.* **2020**, *36*, 453–459. [CrossRef]
35. Amer, S.M.M.; Mikhaylovskaya, A.V.V.; Barkov, R.Y.Y.; Kotov, A.D.D.; Mochugovskiy, A.G.G.; Yakovtseva, O.A.A.; Glavatskikh, M.V.V.; Loginova, I.S.S.; Medvedeva, S.V.V.; Pozdniakov, A.V.V. Effect of Homogenization Treatment Regime on Microstructure, Recrystallization Behavior, Mechanical Properties, and Superplasticity of Al-Cu-Er-Zr Alloy. *JOM* **2021**, *73*, 3092–3101. [CrossRef]
36. Amer, S.M.; Barkov, R.Y.; Pozdniakov, A.V. Effect of Mn on the Phase Composition and Properties of Al–Cu–Y–Zr Alloy. *Phys. Met. Metallogr.* **2020**, *121*, 1227–1232. [CrossRef]
37. Amer, S.; Yakovtseva, O.; Loginova, I.; Medvedeva, S.; Prosviryakov, A.; Bazlov, A.; Barkov, R.; Pozdniakov, A. The Phase Composition and Mechanical Properties of the Novel Precipitation-Strengthening Al-Cu-Er-Mn-Zr Alloy. *Appl. Sci.* **2020**, *10*, 5345. [CrossRef]
38. Amer, S.M.; Barkov, R.Y.; Prosviryakov, A.S.; Pozdniakov, A.V. Structure and Properties of New Heat-Resistant Cast Alloys Based on the Al–Cu–Y and Al–Cu–Er Systems. *Phys. Met. Metallogr.* **2021**, *122*, 908–914. [CrossRef]
39. Amer, S.M.; Barkov, R.Y.; Prosviryakov, A.S.; Pozdniakov, A. V Structure and Properties of New Wrought Al-Cu-Y- and Al-Cu-Er-Based Alloys. *Phys. Met. Metallogr.* **2021**, *122*, 915–922. [CrossRef]
40. Zhong, H.; Li, S.; Wu, J.; Deng, H.; Chen, J.; Yan, N.; Chen, Z.; Duan, L. Effects of retrogression and re-aging treatment on precipitation behavior, mechanical and corrosion properties of a Zr+Er modified Al-Zn-Mg-Cu alloy. *Mater. Charact.* **2022**, *183*, 111617. [CrossRef]
41. Zhang, Z.; Li, D.; Li, S.; Deng, H.; Zhang, S.; Fang, J.; Yuan, H.; Deng, B.; Qi, L. Effect of direct aging treatment on microstructure, mechanical and corrosion properties of a Si-Zr-Er modified Al-Zn-Mg-Cu alloy prepared by selective laser melting technology. *Mater. Charact.* **2022**, *194*, 112459. [CrossRef]

42. Wang, Y.; Wu, X.; Cao, L.; Tong, X.; Couper, M.J.; Liu, Q. Effect of trace Er on the microstructure and properties of Al–Zn–Mg–Cu–Zr alloys during heat treatments. *Mater. Sci. Eng. A* **2020**, *792*, 139807. [CrossRef]
43. Lu, J.-T.; Huang, H.; Wu, H.; Wen, S.-P.; Gao, K.-Y.; Wu, X.-L.; Nie, Z.-R. Mechanical properties and corrosion behavior of a new RRA-treated Al–Zn–Mg–Cu–Er–Zr alloy. *Rare Met.* **2023**, *42*, 672–679. [CrossRef]
44. Huang, Y.; Zhang, C.; Ma, Y.; Liu, Y. Effects of homogenization on the dissolution and precipitation behaviors of intermetallic phase for a Zr and Er containing Al–Zn–Mg–Cu alloy. *Prog. Nat. Sci. Mater. Int.* **2020**, *30*, 47–53. [CrossRef]
45. Li, J.; Zhang, Y.; Li, M.; Hu, Y.; Zeng, Q.; Zhang, P. Effect of combined addition of Zr, Ti and Y on microstructure and tensile properties of an Al-Zn-Mg-Cu alloy. *Mater. Des.* **2022**, *223*, 111129. [CrossRef]
46. Glavatskikh, M.V.; Barkov, R.Y.; Khomutov, M.G.; Pozdniakov, A.V. The Effects of Yttrium and Erbium on the Phase Composition and Aging of the Al–Zn–Mg–Cu–Zr Alloy with a High Copper Content. *Phys. Met. Metallogr.* **2022**, *123*, 617–623. [CrossRef]
47. Glavatskikh, M.V.; Barkov, R.Y.; Khomutov, M.G.P.A.V. Structure and properties of the Al-Zn-Mg-Cu-Zr-Y(Er) alloys sheets doped by manganese. *Phys. Met. Metallogr.* **2023**, *in press*.
48. Pozdniakov, A.V.; Zolotorevskiy, V.S. Determining hot cracking index of Al–Si–Cu–Mg casting alloys calculated using effective solidification range. *Int. J. Cast Met. Res.* **2014**, *27*, 193–198. [CrossRef]
49. Liu, X.; Wang, B.; Li, Q.; Wang, J.; Zhang, C.; Xue, C.; Yang, X.; Tian, G.; Liu, X.; Tang, H. Quantifying the Effects of Grain Refiners Al-Ti-B and La on the Microstructure and Mechanical Properties of W319 Alloy. *Metals* **2022**, *12*, 627. [CrossRef]